

Biquadratic coupling drives magnetic detwinning in EuFe_2As_2

Jannis Maiwald,¹ I. I. Mazin,² and Philipp Gegenwart¹

¹Experimentalphysik VI, Universität Augsburg, Universitätsstraße 1, 86135 Augsburg, Germany

²Code 6393, Naval Research Laboratory, Washington, DC 20375, USA

(Dated: February 3, 2017)

Detwinning of magnetic (nematic) domains in Fe-based superconductors has so far only been obtained through mechanical straining, which considerably perturbs the ground state of these materials. The recently discovered non-mechanical detwinning in EuFe_2As_2 by ultra-low magnetic fields offers an entirely different, non-perturbing way to achieve the same goal. However, this way seemed risky due to the lack of a microscopic understanding of the magnetically driven detwinning. Specifically, the following issues remained unexplained: (i) ultra-low value of the first detwinning field of ~ 0.1 T, two orders of magnitude below that of BaFe_2As_2 , (ii) reversal of the preferential domain orientation at ~ 1 T, and restoration of the low-field orientation above 10–15 T. In this paper, we present, using published as well as newly measured data, a full theory that quantitatively explains all the observations. The key ingredient of this theory is a biquadratic coupling between Fe and Eu spins, analogous to the Fe-Fe biquadratic coupling that drives the nematic transition in this family of materials.

Introduction One of the most admirable experimental feats in studies of Fe-based superconductors (FeBS) is the mechanical detwinning of the low-temperature phases of the parent compounds in the 122 families^{1,2}. This allowed impressive insight into the physics of spin-driven nematicity, a phenomenon that arguably rivals the superconductivity itself in these materials. In this connection, one of the most intriguing and unexpected findings was that this nematic physics is ensured by a sizable biquadratic magnetic interaction, something unheard of in localized magnetic moment systems, and never investigated in itinerant magnetic metals. This phenomenon was first discovered computationally³ and later shown to provide the only physically meaningful description of spin dynamics in FeBS⁴. There is growing evidence that it is not limited to FeBS, but occurs also in other itinerant systems⁵.

Mechanical straining is not the only way to detwin FeBS. It was shown that a static magnetic field of ~ 15 T leads to partial detwinning⁶ and pulsed fields of ~ 30 T to nearly complete detwinning⁷. Later we will analyze these facts in more detail, but at the moment we emphasize that these are relatively large fields, even though the in-plane magnetic anisotropy energy of the FeAs planes was experimentally shown to be of the order of 0.5 meV and, therefore, sizable compared to e.g. elemental Fe, where it is only a few μeV . Against this background, it came as a complete surprise when it was discovered^{8,9} that substituting Ba with Eu lowers the field needed for full detwinning by two orders of magnitude. In principle, this magnetic detwinning allows for a virtually non-intrusive (the energy scale associated with this field is less than 20 mK) investigation of the physics of the nematic state. However, this seemingly exciting opportunity was met with limited enthusiasm for the simple reason that no plausible microscopic explanation could be found for the detwinning itself, given the minuscule amplitude of the required field. Even more striking was the discovery that by increasing the magnetic field gradually one can switch the sign of detwinning *twice*: initially,

magnetic domains tend to orient themselves so that the Fe-Fe long (antiferromagnetic) bonds, oriented along x (crystallographic a) are orthogonal to the applied field (we call this orientation b-domains, because the crystallographic b is aligned with the field). This process is essentially complete at $H_0 \sim 0.5$ T. Then, at $H_1 \sim 1$ T domains spontaneously rotate by 90° , and at $H_2 \sim 10$ T start to turn back to the detwinned state that was initially generated at $H \lesssim 0.5$ T. With such a complex phase diagram, and no theoretical understanding of the underlying phenomena, it is indeed worrisome to embark on systematic studies of nematicity with the risk that unknown magnetic physics may affect the findings. The goal of this paper is to remedy this situation and present a full and quantitative theory explaining all the above observations. It appears that magnetically induced detwinning is intimately related with the nature of the nematicity itself, namely, it is also driven by a sizable biquadratic interaction, which, in turn, is the consequence of the Janusian itinerant-localized nature of the FeBS.

Formalism Let us start with the (simpler) case of BaFe_2As_2 . The minimal approximation is the nearest-neighbor (n.n) Heisenberg model with single site anisotropy:

$$\mathcal{H}_{\text{Fe}} = -\tilde{D} \sum_i f_{i,x}^2 + \tilde{J} \sum_{\langle ij \rangle} \mathbf{f}_i \cdot \mathbf{f}_j - \tilde{M} \sum_i \mathbf{f}_i \cdot \mathbf{H} \quad (1)$$

where i, j label Fe sites, \mathbf{f}_i is the unit vector directed along the Fe magnetic moment at site i , \tilde{M} is its absolute value, and the summation is over all inequivalent n.n bonds¹⁰. \mathbf{H} is the external field in the corresponding energy units. Here and below we use tildes over symbols for Fe-related parameters.

It is known experimentally that the Fe moments lie within the ab plane and are oriented along the longer a -axis (i.e., $\tilde{D} > 0$). Neutron scattering provides estimates for the parameters as $\tilde{J} \sim 30$ meV, $\tilde{D} \approx 0.25$ meV¹¹. Minimizing Eq. (1) with respect to \mathbf{f} , for $\mathbf{H} \parallel y$ (no linear susceptibility appears for $\mathbf{H} \parallel x$) we observe that H generates a canting of the Fe spins away from the x axis

by an angle $\alpha = \sin^{-1}(\tilde{M}H/4J)$, which corresponds to an energy gain of $E = (\tilde{M}H)^2/4\tilde{J}$ per formula unit (f.u.). There are two ways how the system may take advantage of this energy gain, even if the field is along x . First, all Fe spins may rotate from being aligned along x to being predominantly aligned along y . This process is called spin-flop and occurs when $\tilde{J} > \tilde{D}$. Using $\tilde{M} \approx 1\mu_B$ and the above parameters, we estimate $\tilde{H}^{\text{flop}} = 2\sqrt{2\tilde{D}\tilde{J}}/\tilde{M} \approx 11\text{ meV} \approx 135\text{ T}$. Thus, the spin-flop never occurs at typically lab-accessible fields. The other way is to switch an entire “a-domain” (*i.e.*, a domain with ferromagnetic bonds along b) to a “b-domain”. This process is associated with an unknown energy barrier Δ . Given that in the field of $\sim 15\text{ T}$ the Stanford group has observed partial⁶, and in $\sim 30\text{ T}$ nearly full detwinning⁷, we deduce $\Delta \sim E = (\tilde{M}H)^2/4\tilde{J} \approx 0.025\text{ meV/f.u.}$

One can verify these deductions against mechanical detwinning. The latter is an indirect process wherein it is difficult to access the microscopic strain and stress. Reported values for the latter differ from $\sigma = 6\text{--}20\text{ MPa}$ ^{12,13}. Assuming $\sigma = 10\text{ MPa}$ and taking the elastic modulus to be 10 GPa ^{14,15}, we derive a strain of $\varepsilon \approx 0.1\%$. Finally, using the calculated dependence of the total energy on the microscopic strain¹⁶, we find that this strain corresponds to $\Delta \approx 0.01\text{ meV/f.u.}$, which is in agreement with our magnetic estimate.

Yet another estimate can be obtained by considering the stress σ on the unit cell during mechanical detwinning and calculate the energy associated with the displacement δ from $a \parallel \sigma$ to $b \parallel \sigma$. Using the reported lattice parameters of Eu122¹⁷, we arrive at $\delta = 1.6 \times 10^{-12}\text{ m}$. Assuming $\sigma = 6\text{ MPa}$, this leads also to an energy of $\Delta \approx 0.01\text{ meV/f.u.}$

Given that the detwinning energy, according to this theory, depends quadratically on the magnetic moment, and inversely on the exchange constant, one may naively assume that the same mechanism will be operative in EuFe_2As_2 , given that the ordering temperature in the Eu sublattice is much smaller, $T_N = 19\text{ K}$, and the moment much larger, $M = 7\mu_B$, than for the Fe sublattice. Such a phenomenology was adapted in Ref.⁹ in order to parametrize the observed effect. However, it is easy to see that it is microscopically untenable. Indeed, while it is possible and reasonable to write down interactions *inside* the Eu sublattice in Heisenberg form,

$$\mathcal{H}_{Eu} = J_{\parallel} \sum_{\langle ij \rangle} \mathbf{e}_i \cdot \mathbf{e}_j + J_{\perp} \sum_i \mathbf{e}_i \cdot \mathbf{e}_{i^+} - M \sum_i \mathbf{e}_i \cdot \mathbf{H} \quad (2)$$

where i, j label Eu sites, i^+ the opposing Eu site in the next layer, \mathbf{e}_i the unit vectors directed along the Eu magnetic moment M at site i , and the ferromagnetic $J_{\parallel} < 0$ and antiferromagnetic $J_{\perp} > 0$ constants determine the in-plane and interplanar ordering, respectively, it is not possible to describe the interaction between the Fe and Eu subsystems in the same manner, for the simple reason that the Heisenberg exchange field induced by the

Fe planes on the Eu sites is zero by symmetry (and so is even the dipole field). Note that we did not include any single-site anisotropy in Eq. (2), because Eu adopts a valence state of +2 in this system. Due to the closed f -shell, with 7 electrons in the spin-majority channel, Eu^{2+} has zero angular momentum and negligible magnetocrystalline anisotropy. This is confirmed by first principles calculations, presented in the supplement to this letter. Without an interaction between Fe and Eu, there is no physical mechanism by which the Eu spin dynamics may affect the detwinning.

Moreover, even the basic magnetic properties of EuFe_2As_2 cannot be explained within a simple Heisenberg model. Indeed, the magnetic susceptibility of EuFe_2As_2 above T_N is dominated by the Eu spins and well described by a nearly isotropic Curie-Weiss law, in accordance with the previous paragraph. The effective moment has been determined to be $M = 7\mu_B$ with $T_{CW} \approx -20\text{ K}$ ¹⁸. Eq. (2) suggests $k_B T_{CW} = 4J_{\parallel} - 2J_{\perp} \approx 4J_{\parallel}$. Thus the Néel temperature appears to be equal to the mean-field transition temperature of the individual Eu planes. In other words, each Eu plane orders magnetically at the mean-field temperature, not at all suppressed by fluctuations, and immediately at the transition the antiferromagnetic stacking of the individual planes along c is acquired in violation of the Mermin-Wagner theorem.

At this point, it is instructive to look at first principles calculations and what they tell us about J_{\perp} and J_{\parallel} . The former appears to be very small and depends on the value of the Hubbard U used on the Eu f orbitals. This is not surprising, because it is set by the competition between superexchange, proportional to t_{\perp}^2/U , and Schrieffer-Wolff driven¹⁹ double exchange, proportional to $(t_{\text{Eu-Fe}}^2/U)^2 N(0)$, with $N(0)$ the density of states, and t_{\perp} and $t_{\text{Eu-Fe}}$ the effective Eu-Eu and Eu-Fe hopping across the planes. For $U - J = 0$ we get $J_{\perp} = 0.14\text{ meV/Eu}$ (1.6 K) and for $U - J = 5\text{ eV}$ $J_{\perp} = 0.26\text{ meV/Eu}$ (3 K), while $J_{\parallel} = -2\text{ meV}$ (23 K), and -0.8 meV (9 K), respectively. The LDA+ U results (which we believe are closer to reality) correspond to $T_{CW} \sim -34\text{ K}$, and $T_N \approx 4.27J_{\parallel}/[3.12 + \log(J_{\parallel}/J_{\perp})] = 10\text{ K}$ for the Heisenberg model²⁰. Obviously, the former number is too high and the latter too low. However, if we assume that for an as of yet unknown reason the spin dynamics of Eu is described by an *Ising* model, the numbers are much closer. In that case the Néel temperature is quite a bit higher. For our purpose it is enough to interpolate linearly between the $J_{\perp} = 0$ limit ($T_N = 23\text{ K}$) and the 3D limit ($J_{\perp} = J_{\parallel}$, $T_N = 45\text{ K}$). This interpolation gives $T_N = 30\text{ K}$. That is to say, the calculations universally overestimate J 's by 50 %, but otherwise the similarity between T_{CW} and T_N is not surprising. Even though Eu has a closed shell and no single-site anisotropy, the Ising Hamiltonian is relevant in this case, because—as we will show in the following—a sizable biquadratic coupling between the Eu and Fe subsystems is operative in EuFe_2As_2 . Due to the Fe moments, which order around

190 K, the biquadratic interaction favors an alignment of the Eu moments along the Fe direction and hence promotes their Ising character.

It is well established that, unlike correlated insulators, FeBS superconductors have a considerable biquadratic interaction that plays a crucial role in their nematic behavior²¹. Whether this is a universal property of correlated magnetic metals, which simply had not been given proper attention before, or is unique for FeBS is unknown. With this in mind, we have combined the Hamiltonians from Eqs. (1) and (2) in the following way:

$$\begin{aligned} \mathcal{H} = & -\tilde{M} \sum_{\alpha} \mathbf{f}_{\alpha} \cdot \mathbf{H} + \tilde{J} \sum_{\langle \alpha \beta \rangle} \mathbf{f}_{\alpha} \cdot \mathbf{f}_{\beta} - \tilde{D} \sum_{\alpha} f_{\alpha,x}^2 \\ & - M \sum_i \mathbf{e}_i \cdot \mathbf{H} + J_{\perp} \sum_i \mathbf{e}_i \cdot \mathbf{e}_{i+} \\ & - K \sum_{\alpha,n} (\mathbf{f}_{\alpha} \cdot \mathbf{e}_{\alpha+n})^2, \end{aligned} \quad (3)$$

where the Greek subscripts label the Fe sites, Latin the Eu sites, and the last summation runs over all n.n Fe-Eu pairs. Here and below we use tildes over symbols for Fe-related parameters. We have then estimated the biquadratic Eu-Fe coupling term K from LDA+U calculations (see SM), and obtained an estimate of $K \sim 0.4$ meV. Given the uncertainty in the calculations, this

should be taken as evidence that K is not negligible; later we will determine the actual amplitude of K directly from the experiment.

In the Supplementary Information we present detailed derivations of the solutions of Eq. 3 for both possible orientations of the external field with respect to the crystallographic axes, and for all relevant field regimes. The discussion below omits less relevant parts of the full theory, concentrating on rationalizing the actual experimental observations.

Domain energetics We start our discussion in the *low field* regime, that is $0 < H \lesssim H_1$, before considering higher fields. In this regime the Fe single-site anisotropy dominates and Fe spins are always oriented along the crystallographic a axis, and so are, initially, Eu spins. We will distinguish two cases: first, when \mathbf{H} is applied perpendicular to the initial orientation of Eu spins (b-orientation) or, second, parallel to those (a-orientation). In this regime the former is always lower in energy, since the latter has formally zero spin susceptibility. We will characterize the orientation of the Eu and Fe spins by their respective angles φ and $\tilde{\varphi}$ with respect to the external field. Figure 1(a) is drawn for a b-oriented domain, i.e., $a \perp H$. Equation (3) can then be rewritten in terms of these angles (per one formula unit) as

$$\begin{aligned} \mathcal{E} = & -\tilde{M}H(\cos \tilde{\varphi}_1 + \cos \tilde{\varphi}_2) + 2\tilde{J}\cos(\tilde{\varphi}_2 + \tilde{\varphi}_1) - \tilde{D}(\cos^2 \tilde{\alpha}_1 + \cos^2 \tilde{\alpha}_2) \\ & - MH(\cos \varphi_1 + \cos \varphi_2)/2 + J_{\perp} \cos(\varphi_2 + \varphi_1) \\ & - 2K[\cos^2(\varphi_2 - \tilde{\varphi}_2) + \cos^2(\varphi_2 - \tilde{\varphi}_1) + \cos^2(\varphi_1 - \tilde{\varphi}_2) + \cos^2(\varphi_1 - \tilde{\varphi}_1)], \end{aligned} \quad (4)$$

where α 's are the Fe angles measured from the magnetic easy a -axis.

For the b-orientation and low fields $\tilde{\varphi}_2 = \tilde{\varphi}_1 = \pi/2$, $\varphi_1 = \varphi_2 = \varphi$, $\tilde{\alpha}_2 = \tilde{\alpha}_1 = 0$ and we get

$$E_b = -MHf + (2J_{\perp} + 8K)f^2 + E_0, \quad (5)$$

where we have expressed everything in terms of $f = \cos \varphi$ and $E_0 = -2\tilde{J} - 2\tilde{D} - J_{\perp} - 8K$. The equilibrium tilting angle and energy are given by

$$f_b^{\min} = \frac{MH}{4J_{\perp} + 16K} \quad (6)$$

$$E_b^{\min} = -\frac{(MH)^2}{8(J_{\perp} + 4K)} + E_0. \quad (7)$$

The biquadratic term in the definition of E_0 is always trying to minimize the angle between the Fe spins and Eu spins. Thus, if $\pi/4 < \varphi < \pi/2$, Fe spins prefer to orient perpendicular to the field ($\tilde{\varphi} = \pi/2$), and b-twin

domains are always lower in energy. When φ becomes smaller than $\pi/4$, it becomes more favorable to orient Fe spins parallel to the field ($\tilde{\varphi} = 0$), and this is the first critical field H_1 at which the first domain reorientation takes place (note that in this field regime only $\tilde{\varphi} = \pi/2$ or 0 is allowed, any intermediate value of $\tilde{\varphi}$ is severely punished by the Fe-Fe exchange and single-site anisotropy).

After this orientation has occurred, the total energy is expressed as

$$E_a = -MHf + (2J_{\perp} - 8K)f^2 + E_0 + 8K \quad (8)$$

and consequently

$$f_a^{\min} = \frac{MH}{4J_{\perp} - 16K} \quad (9)$$

$$E_a^{\min} = -\frac{(MH)^2}{8(J_{\perp} - 4K)} + E_0 + 8K. \quad (10)$$

Thus the first reorientation field H_1 is defined by $E_a^{\min} =$

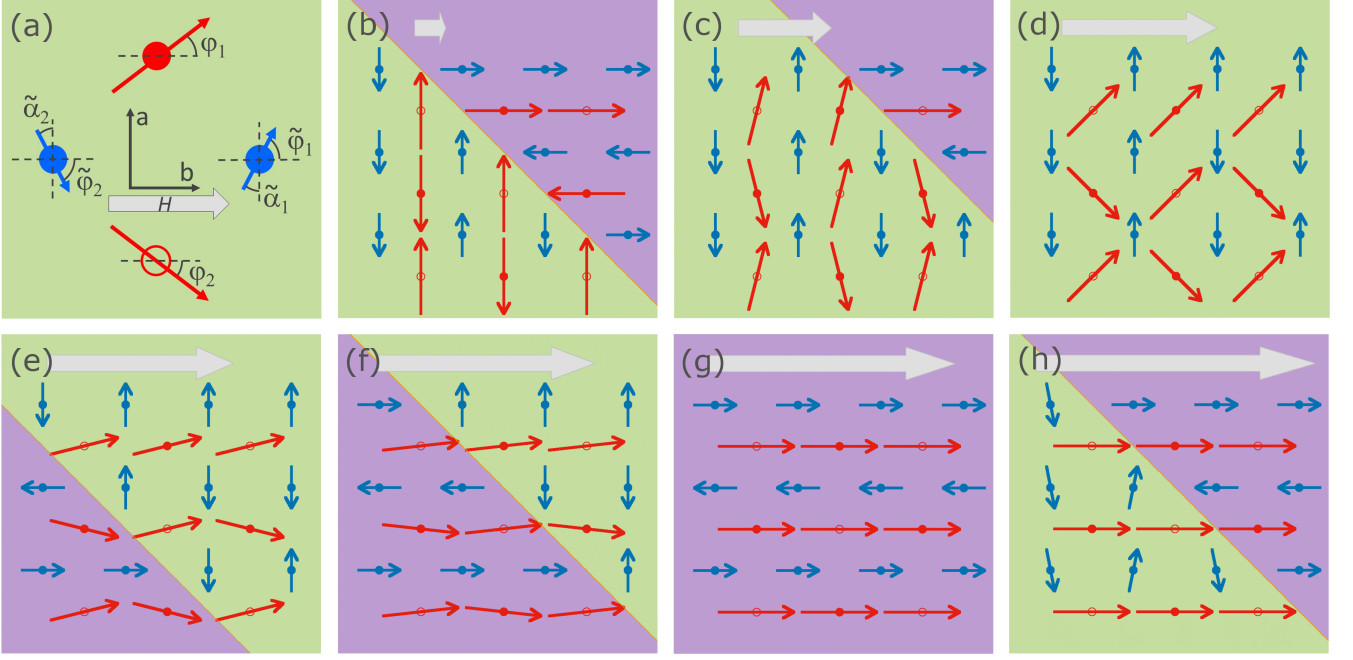


Figure 1: Illustration of the spin [Fe (blue), Eu (red); open circles indicate Eu atoms and spins in the next layer] and domain [b-twin (green), a-twin (violet)] dynamics of EuFe_2As_2 for an (from left to right, increasing) external magnetic field (gray arrow) $H \parallel [110]_T$. (a) Definition of the spin angles. (b) Initial twin distribution at $H = 0$. (c) The b-twins grow with increasing field until (d) at H_0 the system is completely detwinned with $b \parallel H$. (e) Above H_0 the a reorientation to a-twin sets in, (f) which is largest at H_1 and (g) completes above, with $a \parallel H$. (h) Around H_3 the second reorientation back to b-twin occurs.

E_b^{\min} , or

$$H_1 = \frac{2}{M} \sqrt{2(J_{\perp}^2 - 16K^2)} \quad (11)$$

At the field $H_a^{\text{sat}} = 4(J_{\perp} - 4K)/M$ the angle φ becomes 0, that is to say, Eu spins are perfectly aligned with the field. Further increase of the field does not change the total energy (aside from the Zeeman term $-MH$), because from that point on the differential spin susceptibility of the Eu subsystem becomes zero. However, while theoretically important, this field does not manifest itself as a change of regime in domain dynamics.

H_a^{sat} is too small to incur any Fe spin dynamics, but, in principle, with further increase of H one needs to include the spin susceptibility of the Fe subsystem. The latter is zero as long as Fe spins are parallel to Eu spins, satisfying the biquadratic coupling. Yet, in a sufficiently strong field, i.e. at $H \gtrsim H_2$ a potential energy gain from allowing Fe spins to screen the field outweighs the loss of the biquadratic interaction. Mathematically, the latter, in this regime $H > H_a^{\text{sat}}$, is reduced to an effective single-site anisotropy for the Fe subsystem, subtracting from the actual anisotropy, and the transition in question is described by the same formulas as a typical spin-flop transition. We can find the corresponding field value in the same way as one derives the spin-flop field in textbooks: we need the energy gain from the Fe spin-flop

to overcome the energy loss due to noncollinearity (the loss occurs both due to the Fe-Fe exchange \tilde{J} and because the Fe site-anisotropy is much larger than the bi-quadratic coupling).

In this case, the total energy (since now $\varphi = 0$, $\tilde{\alpha} = \pi/2 - \tilde{\varphi}$) is

$$\tilde{E}_b = -2\tilde{M}Hf + 2(2\tilde{J} + \tilde{D} - 4K)f^2 - MH + E_0 + 2J_{\perp} + 8K,$$

where we have now used $f = \cos \tilde{\varphi}$ and E_0 . Minimizing with respect to f yields:

$$f_b^{\min} = \frac{\tilde{M}H}{2(2\tilde{J} + \tilde{D} - 4K)},$$

with the energy gain compared to Eq. 8 with $f = 1$ being

$$dE = + \frac{(\tilde{M}H)^2}{2(2\tilde{J} + \tilde{D} - 4K)} - 8K.$$

This expression changes sign at $H_2 = 4\sqrt{2\tilde{J}K + \tilde{D}K - 4K^2}/\tilde{M} \approx 4\sqrt{2\tilde{J}K}/\tilde{M}$. This is the second critical field at which the reorientation back to the b-domains is initiated.

The domain dynamics, with the first detwinning at H_0 , second (reversed) detwinning at H_1 , and third detwinning at H_2 is illustrated in Fig. 1(b-h) and also in the

movie ([url](#)). There, we depict how Eu and Fe spins (and the structural axes follow the latter) rotate in an external field. One can see that, despite the physical simplicity, the actual dynamics are rather complicated.

Determination of the Coupling Constants While the $H_{0,1,2}$ defined above directly manifest themselves in the experiment, the actual expression for the energy difference between the two types of domains (which is needed to describe domain dynamics, as opposed to thermodynamic equilibrium) is a complicated piecewise function of the field. The full derivation can be found in the Supplement, where explicit expressions for all critical fields are obtained. In the relevant field range for the experiments discussed here this function is given by

$$dE = \begin{cases} \frac{M^2 H^2}{8(J_\perp + 4K)}, & \{0, H_a^{\text{flop}}\} \\ K(8 - \frac{M^2 H^2}{J_\perp^2 - 16K^2}), & \{H_a^{\text{flop}}, H_a^{\text{sat}}\} \\ -MH + 2J_\perp + \frac{M^2 H^2}{8(J_\perp + 4K)}, & \{H_a^{\text{sat}}, H_b^{\text{sat}}\} \\ -8K + \frac{M^2 H^2}{2(2J_\perp - 4K)}, & \{H_b^{\text{sat}}, H_2\}. \end{cases} \quad (12)$$

In the second case $dE > 0$ changes to $dE < 0$ at H_1 , which lies between H_a^{flop} and H_a^{sat} . The fields H_1 , H_a^{sat} and H_2 have been derived above. The transformations associated with H_a^{flop} and H_b^{sat} occur in “wrong”, or minority domains, which are thermodynamically unstable, but occur kinetically. Their expressions, as derived in the Supplement, are $H_b^{\text{sat}} = 4(J_\perp + 4K)/M$ and $H_a^{\text{flop}} = 8/M\sqrt{K(J_\perp - 4K)}$.

The coupling constants J_\perp and K can be determined from experiment. Magnetization, magnetostriction, neutron and magneto-transport measurements, for instance, all can be used to estimate the domain population ratio. In the following we will determine the coupling constants using new magnetization data⁹, and then use them to calculate this ratio as a function of field in order to compare it to the experiment.

When measured along the tetragonal $[110]_T$ direction, a roughly linear magnetization $M(H)$ was reported in Ref.⁹, interrupted only by two pronounced jumps around 0.1 T and 0.6 T. Saturation sets in above 0.9 T with $M \approx 5 \mu_B$. Due to the uncharacteristically small saturated moment, which does not agree well with previously published data¹⁸ and the theoretically expected value of $M = 7 \mu_B$, we have re-measured the magnetization of a EuFe_2As_2 sample from Zapf et al.⁹. The results are shown in Fig. 2 for decreasing magnetic field. The overall behavior is similar, but we found a saturation magnetization of $6.82 \mu_B$, in good agreement with the theoretical expectations and with Ref.¹⁸.

The step-like increase of the magnetization around $0.65 \mu_B \text{ T}$ was associated with a spin-flip transition of the Eu^{2+} moments in Ref.⁹. However, magnetostriction, magneto-transport and unpublished neutron diffraction data indicate that the feature is associated with the re-orientation of domains, rather than an intrinsic spin-flip of the a-twin domain and must, therefore, be identified with H_1 . Furthermore, the Eu saturation field of the b-

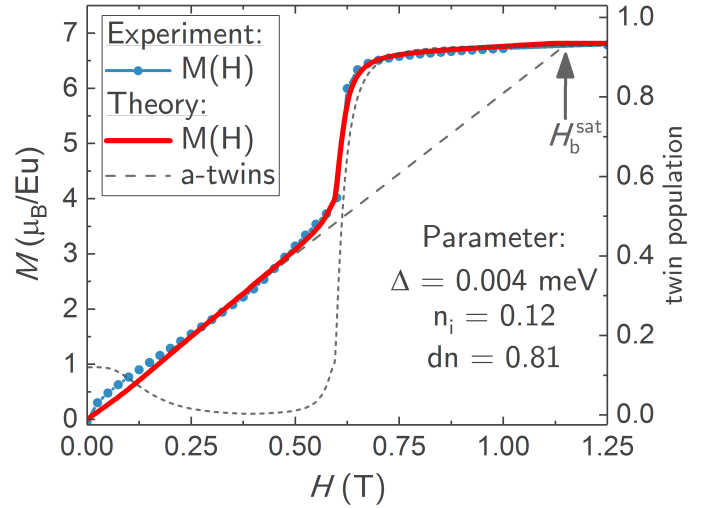


Figure 2: Magnetization at ($T = 5 \text{ K}$) as a function of decreasing magnetic field applied along the $[110]_T$ direction (blue symbols) remeasured from Zapf et al.⁹. The solid line (red) represents our theoretical prediction using the determined coupling constants. The short dashed line depicts the a-twin domain distribution derived from a fit to the corresponding magneto-resistance data, similar to Fig. 5, yielding: $\Delta = 0.004 \text{ meV}$, $n_i = 0.12$ and $dn = 0.81$ (see Supplement). The long dashed line depicts the extrapolation of H_b^{sat} , as discussed in the text.

twin domain can be extrapolated to $H_b^{\text{sat}} \approx 1.14 \text{ T}$ from the slope of the low-field region between 0.2 T and 0.5 T (Fig. 2); note that this field needs to be extrapolated, and cannot be measured directly because at $H \gtrsim 1 \text{ T}$ nearly all domains are of the a-type. The constants can be extracted from these two fields as follows:

$$\begin{aligned} J_\perp &= \frac{M}{8} H_b^{\text{sat}} \left[1 + 2 \left(\frac{H_1}{H_b^{\text{sat}}} \right)^2 \right] \\ K &= \frac{M}{32} H_b^{\text{sat}} \left[1 - 2 \left(\frac{H_1}{H_b^{\text{sat}}} \right)^2 \right]. \end{aligned} \quad (13)$$

The results are shown (Sample 1) in Tab. (SII) in the supplement. We have cross-checked the results by using parameters determined from various samples grown with different techniques and other measurements like magnetostriction, magneto-transport and unpublished neutron data. The results appear to be consistent between measurements, but we found a noticeable sample dependence, which also seems to be related to the synthesis methods of the single crystals, see also Tab. (SII). The averaged values are $J_\perp = 0.122(2) \text{ meV}$, $K = 0.0077(33) \text{ meV}$ and $J_\perp/K \approx 18(6)$.

Energy barrier and domain dynamics The domain dynamics is driven by the energy difference dE between the domains. In Fig. 3 we show dE on a semi-log plot as a function of the reduced variable MH/J_\perp for a representative ratio of $K/J_\perp = 0.05$. Positive values correspond to the b-twin domain being the ground state,

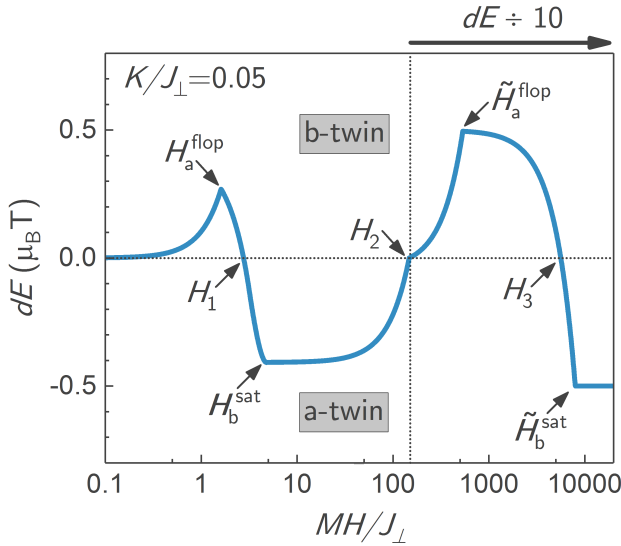


Figure 3: Calculated domain energy difference dE as a function of MH/J_{\perp} for of a characteristic ratio of $K/J_{\perp} = 0.05$. For better visibility, values above H_2 (vertical dashed line) are rescaled by a factor of 10. Positive values and negative values correspond to the b-twin and a-twin domain, respectively. The horizontal dashed line indicates $dE = 0$.

while for negative ones the a-twin is the ground state. The phase diagram in a large parameter space in reduced coordinates $\{K/J_{\perp}, MH/J_{\perp}\}$ is shown in Fig. 4. The remainder of the formulas used in constructing this phase diagram can be found in the supplement.

Until now we have assumed that the reorientation of twin domains has no energy cost. In reality, however, there is an unknown energy barrier Δ associated with the reorientation, i.e. the energy difference $dE = E_{a\text{-twin}} - E_{b\text{-twin}}$ between the two twin variants needs to exceed a certain threshold before reorientation occurs. In the following, we will assume Δ for various domain walls to be log-normal distributed, i.e. $\log \Delta$ is normal²². This is a typical distribution of grain sizes in polycrystalline matter²³. The cumulative distribution function $F_X(x)$ of a positive log-normal distributed variable X is given by $F_X(x) = \frac{1}{2} \operatorname{erfc}\left(-\frac{\log x - \mu}{\sigma\sqrt{2}}\right)$, with the location and the scaling parameters μ and σ . Due to the fact that dE changes sign as a function of applied field, the log-normal distribution in our case generates the following fitting function:

$$y = \begin{cases} n_0 \cdot \frac{1}{2} \operatorname{erfc}\left(\frac{\log(dE/\Delta)}{\sqrt{2}}\right), & dE > 0 \\ dn \cdot \frac{1}{2} \operatorname{erfc}\left(-\frac{\log(-dE/\Delta)}{\sqrt{2}}\right) + n_0, & dE < 0 \end{cases},$$

with n_0 the fraction of a-twin domains at $H = 0$ and $dn = n_{\text{sat}} - n_0$ the difference between the saturated a-twins n_{sat} and n_0 . Together with Eq. 12 this function fully describes the domains distribution.

Prior to performing the fit, the domain population needs to be extracted from the available measurements.

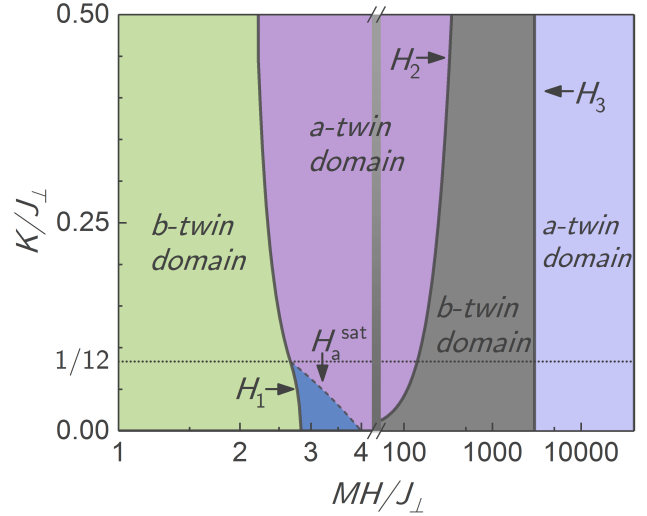


Figure 4: Phase diagram K/J_{\perp} vs. MH/J_{\perp} in thermodynamic equilibrium. The four phases shown correspond to: The b-twin domains (green) with canted Eu^{2+} spins, a-twin domains with saturated (purple) or unsaturated (blue) Eu magnetization, respectively, followed by the b-twin domains (gray) induced by the canting of Fe spins. Finally another hypothetical phase of a-twin domains, induced by further canting of the Fe spins, is shown (light blue). More details, also on the significance of the dotted line, indicating $12K/J_{\perp} = 1$, can be found in the Supplement.

The domain population $n(H)$ can be determined in a variety of ways. Arguably the most exact data can be extracted from field-dependent neutron diffraction measurements on a free standing sample, which will be published soon²⁴. In the following we will use magnetostriction (MS) data by Zapf et al.⁹, which agree with the preliminary data of Ref.²⁴.

The MS is defined as $\Delta L(H)/L_0 = (L(H) - L_0)/L_0$, where L_0 and $L(H)$ are the initial and field-dependent average unit cell length, respectively. They can be expressed by $L(H) = n(H)a + [1 - n(H)]b$ and $L_0 = n_0a + (1 - n_0)b$, again with the (initial) domain population n_0 at $H = 0$ and orthorhombic lattice parameters a and b . Solving for n leads to

$$n(H) = \frac{\Delta L}{L_0} \left(\frac{b}{a - b} + n_0 \right),$$

from which

$$n_0 = \frac{a \cdot n(H) - b[n(H) + \Delta L/L_0]}{(a - b)(1 + \Delta L/L_0)}, \quad (14)$$

assuming full detwinning at the observed minimum around H_a^{flop} , with $b \parallel H$, i.e. $n(H_a^{\text{flop}}) = 0$. This assumption is justified, as preliminary neutron data²⁴ indicate a domain distribution with $n(H_a^{\text{flop}}) = 0.06$. Furthermore, the significant pressure of the dilatometer in field direction, 1.35 MPa⁹ aids the $n = 0$ alignment at small magnetic fields (but hinders it at larger fields, when $n \rightarrow 1$).

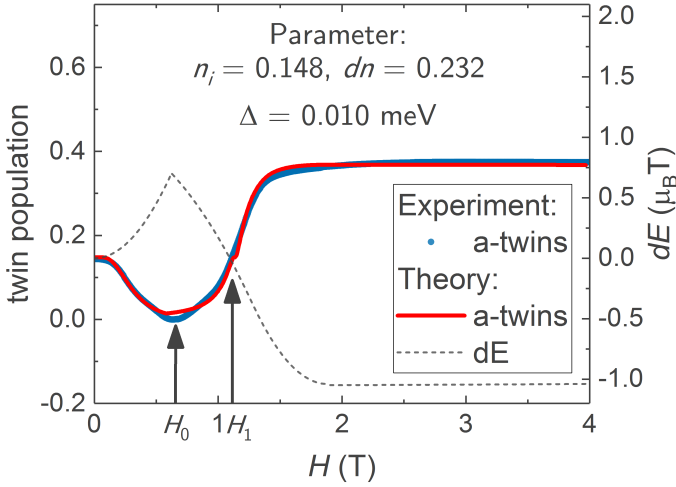


Figure 5: Twin domain population derived from magnetostriction data at ($T = 5K$) from Ref.⁹ as a function of (increasing) magnetic field applied along the $[110]_T$ direction (blue line) as discussed in the main text. The solid line (red) represents the theoretical prediction using the constants' values derived in the main text and the Supplement (see Tab. SII, #2). The dashed line (gray) depicts the theoretically derived domain energy difference dE similar to Fig. 3(b). The a-twin domain population is reduced, due to the pressure of the dilatometer, which favors the b-twin domain in this orientation.

The extracted domain population is shown in Fig. 5. The solid red line represents the fit to the data (blue symbols). The energy barrier for this particular sample and measurement technique is $\Delta = 0.01$ meV. Among the other investigated samples Δ ranges roughly between 10^{-3} meV and 10^{-2} meV, in agreement with the estimates presented in the introduction.

Consistency check

Using the averaged constants from the previous paragraph we find $H_1 = 0.85$ T and $H_2 = 35$ T, in very good agreement with experiment. Utilizing the knowledge about the energy barrier, we can calculate the first detwinning field from the condition $dE = \Delta$, through

$$H_0 = \frac{2}{M} \sqrt{2\Delta(J_{\perp} + 4K)}.$$

For the determined range between 0.001 meV and 0.01 meV this yields 0.09 T to 0.28 T which is also in excellent agreement with the experimental evidence.

Going even further, the presented theory allows us to calculate our new magnetization data, by weighting the Eu magnetization of the twin sublattices with the domain distribution (dashed line) $n(H)$, that we calculated using $\Delta = 0.004$ meV, $n_i = 0.22$ and $dn = 0.71$. The total magnetization is given by

$$M(H) = n(H) \cdot M_a + (1 - n(H)) \cdot M_b,$$

where M_a and M_b are the magnetization of the sublattices

given by $M \cos \varphi$, i.e.

$$M_a = \begin{cases} 0, & \{0, H_a^{\text{flop}}\} \\ \frac{M^2 H}{4(J_{\perp} - 4K)}, & \{H_a^{\text{flop}}, H_a^{\text{sat}}\} \\ M, & \{H_a^{\text{sat}}, \infty\}, \end{cases}$$

$$M_b = \begin{cases} \frac{M^2 H}{4(J_{\perp} + 4K)}, & \{0, H_b^{\text{sat}}\} \\ M, & \{H_b^{\text{sat}}, \infty\}. \end{cases}$$

The result of the simulation is depicted by the solid red line in Fig. 2.

Summary We present a microscopic, physically meaningful and quantitative description of the observed magnetic detwinning effect in FeBS, with all its complexity. In particular, the following mysteries have been resolved: (i) strong detwinning in minuscule fields despite absence of spin-orbit coupling effects in Eu^{2+} ions; (ii) coupling of Eu spin orientation to the Fe sublattice, despite any bilinear interaction canceling out by symmetry, and (iii) double reversal of the preferential domain orientation with the increase of the external field. We show that all these issues find a natural explanation if a *bi-quadratic* Eu-Fe coupling is included in the model. We also show that such a term does actually appear in first-principles calculation, with an amplitude even stronger than needed to explain the experimental data. Furthermore, we were able to describe quantitatively not only the thermodynamic phase diagram, but even the dynamics of detwinning (as deduced from our new magnetization data), assuming that the detwinning energy barriers are distributed according the log-normal law (quite typical in crystal morphology). Such a microscopic physical understanding of the phenomenon of magnetic detwinning in ultra-low magnetic fields opens new avenues for studying experimentally the spin-driven nematicity in Fe-based superconductors.

Acknowledgments

We are grateful to Shibabrata Nandi and Yinguo Xiao for giving us access to their neutron diffraction data, to Makariy Tanatar for sharing with us his data on mechanical detwinning and to Ian Fisher for discussing with us the concept of this work. We also like to convey our gratitude to Shuai Jiang, Christian Stingl and Jeevan H.S. for permitting us access to their samples and magnetostriction data and Sina Zapf and Martin Dressel for collaboration in the early stage of this project (Ref.⁹). J.M. thanks Patrick Seiler for support and discussions. J.M. and P.G. are supported by DFG through SPP 1458. I.I.M. is supported by ONR through the NRL basic research program.

Author contributions

J.M. carried out the sample preparation and experimental measurements. I.I.M. performed the first principles calculations. J.M. and I.I.M. participated equally in the development of the theory and in writing the manuscript. P.G. supervised the project on the Augsburg side.

Additional information
Supplementary Information accompanies this paper.

Competing financial interests: The authors declare no competing financial interests.

- ¹ Fisher, I. R., Degiorgi, L. & Shen, Z. X. In-plane electronic anisotropy of underdoped '122' Fe-arsenide superconductors revealed by measurements of detwinned single crystal. *Rep. Prog. Phys.* **74**, 124506 (2011).
- ² Tanatar, M. A., Kreyssig, A., Nandi, S., Ni, N., Bud'ko, S. L., Canfield, P. C., Goldman, A. I. & Prozorov, R. Direct imaging of the structural domains in the iron pnictides $A\text{Fe}_2\text{As}_2$ ($A = \text{Ca}, \text{Sr}, \text{Ba}$). *Phys. Rev. B* **79**, 180508(R) (2009).
- ³ Yaresko, A. N., Liu, G.-Q., Antonov, V. N. & Andersen, O. K. Interplay between magnetic properties and Fermi surface nesting in iron pnictides. *Phys. Rev. B* **79**, 144421 (2009).
- ⁴ Wysocki, A. L., Belashchenko, K. D. & Antropov, V. P. Consistent model of magnetism in ferropnictides. *Nat. Phys.* **7**, 485–489 (2011).
- ⁵ Zhang, G., Glasbrenner, J. K., Flint, R., Mazin, I. I. & Fernandes, R. M., to be published.
- ⁶ Chu, J.-H., Analytis, J. G., Press, D., De Greve, K., Ladd, T. D., Yamamoto, Y. & Fisher, I. R. In-plane electronic anisotropy in underdoped $\text{Ba}(\text{Fe}_{1-x}\text{Co}_x)_2\text{As}_2$ revealed by partial detwinning in a magnetic field. *Phys. Rev. B* **81**, 214502 (2010).
- ⁷ Ruff, J. P. C., Chu, J.-H., Kuo, H.-H., Das, R. K., Nojiri, H., Fisher, I. R. & Islam, Z. Susceptibility Anisotropy in an Iron Arsenide Superconductor Revealed by X-Ray Diffraction in Pulsed Magnetic Fields. *Phys. Rev. Lett.* **109**, 027004 (2012).
- ⁸ Xiao, Y., Su, Y., Schmidt, W., Schmalzl, K., Kumar, C. M. N., Price, S., Chatterji, T., Mittal, R., Chang, L. J., Nandi, S., Kumar, N., Dhar, S. K., Thamizhavel, A. & Brueckel, Th. Field-induced spin reorientation and giant spin-lattice coupling in EuFe_2As_2 . *Phys. Rev. B* **81**, 220406 (2010).
- ⁹ Zapf, S., Stingl, C., Post, K. W., Maiwald, J., Bach, N., Pietsch, I., Neubauer, D., Löhle, A., Clauss, C., Jiang, S., Jeevan, H. S., Basov, D. N., Gegenwart, P. & Dressel, M. Persistent Detwinning of Iron-Pnictide EuFe_2As_2 Crystals by Small External Magnetic Fields. *Phys. Rev. Lett.* **113**, 227001 (2014).
- ¹⁰ It is well established that a microscopically justifiable model includes Heisenberg terms up to the third neighbors and a sizable n.n biquadratic coupling⁴, but for our purpose of calculating the spin canting in an external magnetic field and the corresponding energy gain, all this complexity can be absorbed in one parameter, of which we only need to know the order of magnitude.
- ¹¹ Wang, C., Zhang, R., Wang, F., Luo, H., Regnault, L. P., Dai, P. & Li, Y. Longitudinal Spin Excitations and Magnetic Anisotropy in Antiferromagnetically Ordered BaFe_2As_2 . *Phys. Rev. X* **3**, 041036 (2013).
- ¹² Jiang, S., Jeevan, H. S., Dong, J. & Gegenwart, P. Thermopower as a Sensitive Probe of Electronic Nematicity in Iron Pnictides. *Phys. Rev. Lett.* **110**, 067001 (2013).
- ¹³ Blomberg, E. C., Kreyssig, A., Tanatar, M. A., Fernandes, R. M., Kim, M. G., Thaler, A., Schmalian, J., Bud'ko, S. L., Canfield, P. C., Goldman, A. I. & Prozorov, R. Effect of tensile stress on the in-plane resistivity anisotropy in BaFe_2As_2 . *Phys. Rev. B* **85**, 144509 (2012).
- ¹⁴ Shein, I. R. & Ivanovskii, A. L. Elastic properties and chemical bonding in ternary arsenide SrFe_2As_2 and quaternary oxyarsenide LaFeAsO – Basic phases for new 38-55 K superconductors from first principles. *Physica C* **469**, 1230011 (2009).
- ¹⁵ Yoshizawa, M. & Simayi, S. Anomalous Elastic Behavior and its Correlation with Superconductivity in Iron-Based Superconductor $\text{Ba}(\text{Fe}_{1-x}\text{Co}_x)_2\text{As}_2$. *Mod. Phys. Lett. B* **26**, 15-19 (2012).
- ¹⁶ Jesche, A., Caroca-Canales, N., Rosner, H., Borrmann, H., Ormeci, A., Kasinathan, D., Klauss, H. H., Luetkens, H., Khasanov, R., Amato, A., Hoser, A., Kaneko, K., Krellner, C. & Geibel, C. Strong coupling between magnetic and structural order parameters in SrFe_2As_2 . *Phys. Rev. B* **78**, 180504(R) (2008).
- ¹⁷ Xiao, Y., Su, Y., Meven, M., Mittal, R., Kumar, C. M. N., Chatterji, T., Price, S., Persson, J., Kumar, N., Dhar, S. K., Thamizhavel, A. & Brueckel, Th. Magnetic structure of EuFe_2As_2 determined by single-crystal neutron diffraction. *Phys. Rev. B* **80**, 174424 (2009).
- ¹⁸ Jiang, S., Luo, Y., Ren, Z., Zhu, Z., Wang, C., Xu, X., Tao, Q., Cao, G. & Xu, Z. Metamagnetic transition in EuFe_2As_2 single crystals. *New J. Phys.* **11**, 025007 (2009).
- ¹⁹ Glasbrenner, J. K., Žutić, I. & Mazin, I. I. Theory of Mn-doped II-II-V semiconductors. *Phys. Rev. B* **90**, 140403(R) (2014).
- ²⁰ C. Yasuda, S. Todo, K. Hukushima, F. Alet, M. Keller, M. Troyer, and H. Takayama, *Phys. Rev. Lett.* **94**, 217201 (2005).
- ²¹ Glasbrenner, J. K., Mazin, I. I., Jeschke, H. O., Hirschfeld, P. J., Fernandes, R. M. & Valenti, R. Effect of magnetic frustration on nematicity and superconductivity in iron chalcogenides. *Nat. Phys.* **11**, 953-958 (2015).
- ²² Limpert, E., Stahel, W. A. & Abbt, M. Log-normal Distributions across the Sciences: Keys and Clues. *BioScience* **51**, 341-352 (2001).
- ²³ *The Quantitative Description of the Microstructure of Materials*, K. J. Kurzydowski, B. Ralph. CRC Press, Boca Raton, 1995
- ²⁴ Maiwald, J., Xiao, Y. & Nandi, S., to be published.

Biquadratic coupling drives magnetic detwinning in EuFe_2As_2 – Supplementary Information –

Jannis Maiwald,¹ I. I. Mazin,² and Philipp Gegenwart¹

¹Experimentalphysik VI, Universität Augsburg, Universitätsstraße 1, 86135 Augsburg, Germany

²Code 6393, Naval Research Laboratory, Washington, DC 20375, USA

(Dated: February 3, 2017)

I. METHODS

A. Computations

In order to estimate computationally the key parameters of the theory (keeping in mind that the final values would be extracted from the experiment), we have performed calculations using the plane wave code VASP¹ with the setup as described in Ref.², and using the Generalized Gradient Approximation (GGA) to the Density Functional Theory (DFT). We have performed two sets of calculations: one with Fe spins along the easy axis a , and Eu spins either parallel or perpendicular to the former, and then taking the energy difference, or with Fe spins along the b , and Eu spins either parallel or perpendicular to the former, and again taking the energy difference. Not unexpectedly, the result depends on the Hubbard U , but for the same U is consistent between two sets. In particular, for $U - J = 7$ eV, we found $K \approx 0.4$ meV, and without U a larger value of ≈ 0.8 meV. Compared to the values extracted from the experiment, these numbers are too large, possibly because the GGA underestimates the wave function localization, and the biquadratic term we are looking for depends on the small overlap of the Eu f and Fe d orbitals, which is very sensitive to localization. Similarly, for estimating J_\perp we compared the total energies of ferromagnetic Eu planes, stacked ferromagnetically or antiferromagnetically along c . Finally, for estimating J_\parallel we compared ferromagnetic and checkerboard-antiferromagnetic in-plane arrangements of Eu ions, always allowing stripe antiferromagnetism for Eu. All these patterns are illustrated in Fig. S1.

B. Experiment

Single crystals of EuFe_2As_2 were grown using three different techniques, namely, Fe-As self-flux³, Sn-flux and the Bridgman method⁴. The respective sample preparation methods were similar to those in the corresponding references. Samples were characterized using energy-dispersive x-ray analysis and x-ray diffraction to confirm composition and structure. Afterwards, they were oriented using a Laue camera and subsequently cut along the tetragonal $[110]_T$ -direction with an electric spark erosion technique. Typical dimensions after cutting were approximately $2 \times 1 \times 0.1$ mm³.

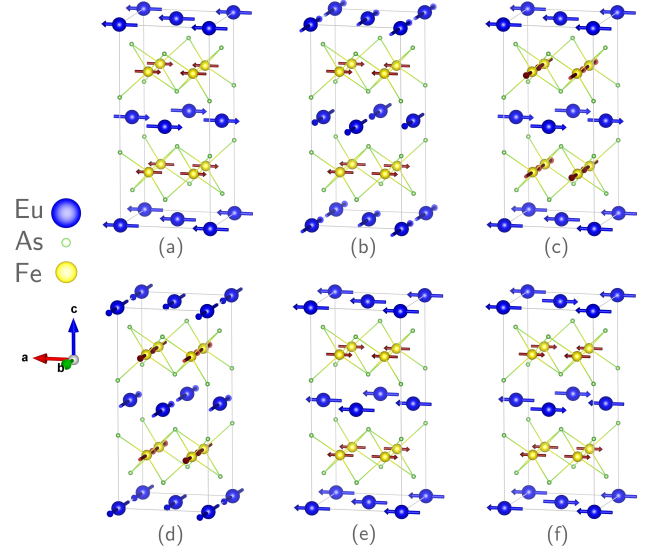


Figure S1: Patterns used for estimating the model parameters from DFT calculations: pattern pairs (a,b) and (c,d) were used for estimating K , pairs (a,e) for J_\perp , and (a,d) for J_\parallel .

Magnetization measurements were performed in a standard Magnetic Property Measurements System (MPMS), while DC-transport data was recorded using a standard Physical Property Measurement System (PPMS) in the Montgomery geometry.

II. MODEL DETAILS

In the main text, we have determined the *equilibrium* phase diagram. Here, we shall derive the energies of each type of domains for all fields, so as to be able to deduce the energy cost/gain of any reorientation. Eq. 12 in the main text is based on this derivation. We will also present, for completeness, the energetics at ultrahigh fields, not accessible in current experiments.

We start from Eq.4 of the main text, and will first calculate the energy of the b-domain ($\mathbf{H} \parallel b$, where b is the hard axis), and then of the a-domain, in all fields. We will consider separately two different regimes: first, small fields compared to the H_2 field defined in the main text, and second, large fields comparable with, or larger than H_2 . In the former regime we can safely neglect the

Fe spins' canting ($\tilde{\varphi}_2 = \tilde{\varphi}_1 = \pi/2$, $\tilde{\alpha}_2 = \tilde{\alpha}_1 = 0$, while in the latter we can use the fact that the Eu magnetization is already saturated and $\varphi_1 = \varphi_2 = 0$).

A. b-Domain: $H \parallel b$.

1. Small Fields

At *small fields* we have, $\tilde{\varphi}_2 = \tilde{\varphi}_1 = \pi/2$, $\tilde{\alpha}_2 = \tilde{\alpha}_1 = 0$ and $\varphi = \varphi_1 = \varphi_2$, which, when inserted into Eq. (4) of the main text leads to

$$\begin{aligned} E_b &= -MH \cos \varphi + J_\perp \cos 2\varphi - 8K \sin^2 \varphi - 2\tilde{J} - 2\tilde{D} \\ &= -MHf + (2J_\perp + 8K)f^2 + E_0, \end{aligned} \quad (1)$$

with $f = \cos \varphi$ and $E_0 = -2\tilde{J} - 2\tilde{D} - J_\perp - 8K$. Minimizing Eq. (1) with respect to f , leads for $MH < 4(J_\perp + 4K)$ to the equilibrium tilting angle and energy given in Eq. (6-7) of the main text. For sufficiently small magnetic fields this solution is always below E_0 and Eu^{2+} moments can screen the field continuously. The tilting angle φ changes gradually according to $\varphi = \cos^{-1}[MH/(4J_\perp + 16K)]$. At fields larger than $H_b^{\text{sat}} = (4J_\perp + 16K)/M$ (derived from $f = 1$) the moments are fully aligned with the external magnetic field and the energy changes to

$$E_b^{\text{sat}} = -MH + 2J_\perp + E_0 + 8K. \quad (2)$$

2. Large Fields

At considerably higher fields the Fe moments will start to deflect ($\tilde{\alpha} = \pi/2 - \tilde{\varphi}$) from the ground state orientation, while the Eu^{2+} moments are already saturated. In this case Eq. (4) of the main text yields

$$\begin{aligned} \tilde{E}_b &= -2\tilde{M}H \cos \tilde{\varphi} + 2\tilde{J} \cos 2\tilde{\varphi} - 2\tilde{D} \sin^2 \tilde{\varphi} \\ &\quad - 8K \cos^2 \tilde{\varphi} - MH + J_\perp \\ &= -2\tilde{M}H\tilde{f} + 2(2\tilde{J} + \tilde{D} - 4K)\tilde{f}^2 \\ &\quad - MH + E_0 + 2J_\perp + 8K \end{aligned}$$

where we have now introduced $\tilde{f} = \cos \tilde{\varphi}$ and E_0 . The equilibrium energy is now determined by minimizing with respect to \tilde{f} , which then reads

$$\tilde{E}_b^{\text{min}} = -MH + 2J_\perp + 8K - \frac{(\tilde{M}H)^2}{2(2\tilde{J} + \tilde{D} - 4K)} + E_0,$$

i.e. Eq. (2) with an additional term stemming from the canting of the Fe moments away from the easy axis.

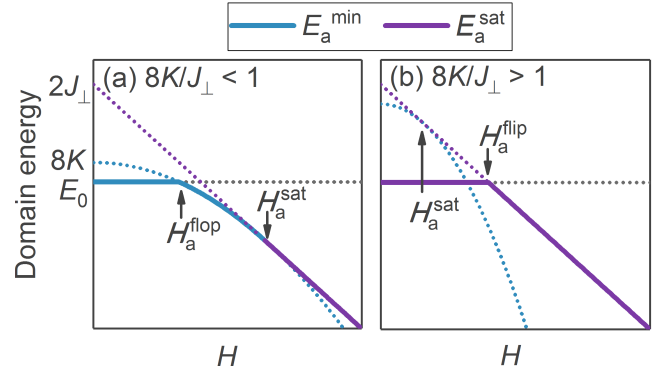


Figure S2: Calculated a-twin domain energy of EuFe_2As_2 as a function of the applied magnetic field for (a) the spin-flop and (b) the spin-flip case.

B. a-Domain: $H \parallel a$

1. Small Fields

At small fields we have the following conditions: $\tilde{\alpha}_1 = \tilde{\varphi}_1 = 0$, $\tilde{\alpha}_2 = \tilde{\varphi}_2 = \pi$ and $\varphi = \varphi_1 = \varphi_2$, leading to

$$\begin{aligned} E_a &= -MH \cos \varphi + J_\perp \cos 2\varphi - 8K \cos^2 \varphi - 2\tilde{J} - 2\tilde{D} \\ &= -MHf + (2J_\perp - 8K)f^2 + E_0 + 8K, \end{aligned}$$

again with $f = \cos \varphi$ and E_0 , which after minimizing w.r.t. f results for $J_\perp > 4K$ and $MH < 4J_\perp - 16K$ in Eqs. (9-10) of the main text. We note the sign change in the denominator and the additional $8K$ -term. Due to this term this state will only be populated once H is large enough. At smaller fields the Eu^{2+} moments will remain in their ground state configuration. The field at which the moments spin-flop $H_a^{\text{flop}} = 8/M\sqrt{K(J_\perp - 4K)}$ is determined from the condition $E_a^{\text{min}} = E_0$. In the spin-flop phase the Eu^{2+} moments gradually rotate towards saturation according to $\varphi = \cos^{-1}[MH/(4J_\perp - 16K)]$. Saturation is reached at $H_a^{\text{sat}} = (4J_\perp - 16K)/M$ at which point the energy in Eq. (10) of the main text changes to

$$E_a^{\text{sat}} = -MH + 2J_\perp + E_0.$$

However, if the biquadratic coupling K is strong compared to the interplanar coupling J_\perp between Eu^{2+} moments, they directly *flip* from the ground state into the fully saturated state, skipping Eq. (10) entirely. Such a spin-flip occurs only if $E_a^{\text{min}}(H_a^{\text{sat}}) \geq E_a^{\text{min}}(H_a^{\text{flop}}) = E_0$, that is to say when $J_\perp \leq 8K$. The corresponding field is then given by $H_a^{\text{flip}} = 2J_\perp/M$. The domain energy of the a-twin for the spin-flop and spin-flip case is shown in Fig. S2.

2. Large field

If the field is large enough the Fe moments can become subject to a spin-flop (but not a spin-flip, because

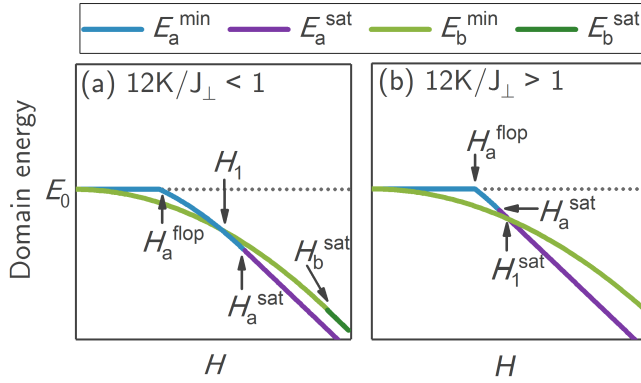


Figure S3: Calculated a-twin and b-twin domain energies of EuFe_2As_2 as a function of the applied magnetic field in two regimes (a) $12K/J_\perp < 1$ and (b) $12K/J_\perp > 1$.

$\tilde{J} \gg \tilde{D}$). As estimated in the main text this should happen around 130 T. We can easily incorporate this effect for the sake of completeness, by setting $\varphi = 0$ and $\tilde{\alpha} = \tilde{\varphi}$, which leads to

$$\begin{aligned} \tilde{E}_a = & -2\tilde{M}H \cos \tilde{\varphi} + 2\tilde{J} \cos 2\tilde{\varphi} - 2\tilde{D} \cos^2 \tilde{\varphi} \\ & - 8K \cos^2 \tilde{\varphi} - MH + J_\perp \end{aligned}$$

and after replacing $\tilde{f} = \cos \tilde{\varphi}$ and E_0 to

$$\begin{aligned} \tilde{E}_a = & -2\tilde{M}H\tilde{f} + 2(2\tilde{J} - \tilde{D} - 4K)\tilde{f}^2 \\ & - MH + E_0 + 2J_\perp + 2\tilde{D} + 8K, \end{aligned}$$

Subsequent minimization w.r.t. f results in

$$\tilde{f}_{\text{flop}}^{\text{min}} = \frac{\tilde{M}H}{2(2\tilde{J} - \tilde{D} - 4K)},$$

and

$$\tilde{E}_a^{\text{min}} = -MH + 2J_\perp - \frac{(\tilde{M}H)^2}{2(2\tilde{J} - \tilde{D} - 4K)} + E_0 + 2\tilde{D} + 8K,$$

where the Fe spin-flop field is given from the condition $\tilde{E}_a^{\text{min}} - E_a^{\text{sat}} = 0$, i.e. $\frac{(\tilde{M}H)^2}{2(2\tilde{J} - \tilde{D} - 4K)} = 2\tilde{D} + 8K$:

$$\tilde{H}_a^{\text{flop}} = \frac{2}{\tilde{M}} \sqrt{(\tilde{D} + 4K)(2\tilde{J} - \tilde{D} - 4K)}$$

In the saturated case it follows from $\tilde{f} = 1$ that

$$\tilde{E}_a^{\text{sat}} = -MH + 2J_\perp - 2\tilde{M}H + 4\tilde{J} + E_0,$$

which becomes valid at the saturation field

$$\tilde{H}_a^{\text{sat}} = \frac{2}{\tilde{M}} (2\tilde{J} - \tilde{D} - 4K).$$

C. Detwinning Dynamics

The full energy map for both types of domains in all fields allows us to calculate the energy cost/gain of switching from a-twin domains to b-twin domains, dE , as a function of the reduced field, MH/J_\perp , and reduced biquadratic coupling, K/J_\perp . While, as discussed in the main text, we have only three experimentally observed phases, their dynamics depends on the energy difference $dE(H)$.

To illustrate this point, we show in Fig. S3 the energy of the two types of domains in the small-field regime for two specific instances of the K/J_\perp ratio. While initially only the b-twin can reduce its energy, leading to the first phase, the energy of the a-twin domain will start to reduce as well once H_a^{flop} or H_a^{flip} (depending on the ratio of K/J_\perp) is reached. Due to the minus sign in the denominator of Eq. (10) of the main text, this reduction is more pronounced than in the b-twin domain, leading to a crossing of the two energies. At this particular point, a domain reorientation from $b \parallel H$ to $a \parallel H$ will be favored. Two cases are evident: if $12K/J_\perp < 1$, E_b^{min} will intersect with E_a^{min} at H_1 , while for $12K/J_\perp > 1$, E_b^{min} crosses with E_a^{sat} at $H_1^{\text{sat}} > H_a^{\text{sat}}$, where

$$H_1^{\text{sat}} = \frac{4}{M} (J_\perp + 4K) \left(1 - \sqrt{\frac{4K}{J_\perp + 4K}} \right), \quad (3)$$

The difference in energy at high fields between E_b^{sat} and E_a^{sat} is set by the biquadratic coupling $8K$. Once the canting of the Fe moments in the b-twin domain is significant, the energy of the b-twin will start to decrease, leading to the reorientation ($E_a^{\text{sat}} = \tilde{E}_b^{\text{min}}$) back to the initial phase, i.e. with $b \parallel H$. The corresponding field is given by

$$H_2 = \frac{4}{\tilde{M}} \sqrt{K(2\tilde{J} + \tilde{D} - 4K)} \approx \frac{4}{\tilde{M}} \sqrt{2K\tilde{J}}.$$

At extremely high magnetic fields the Fe moments can spin-flop, which would lead to a final domain reorientation ($\tilde{E}_b^{\text{min}} = \tilde{E}_a^{\text{min}}$) with $a \parallel H$. The associated field, however, is unphysically large:

$$H_3 = \frac{1}{\tilde{M}} \sqrt{8(\tilde{J} - 2K)^2 - 2\tilde{D}^2} \approx \frac{2}{\tilde{M}} \sqrt{2\tilde{J}} > 1100 \text{ T}.$$

Since the domain dynamics is driven by the energy difference dE between the domains we show in Fig. S4 $dE = E_a - E_b$ on a semi-log color map as a function of the reduced K/J_\perp and MH/J_\perp . The dotted line represents $K/J_\perp = 0.05$, for which dE was depicted in the main text (Fig. 3). Positive and negative values correspond to the b-twin and a-twin domains being the ground state. All fields and regimes are summarized in Table SI for the case $12K/J_\perp < 1$.

Table **SI**: The energy difference dE in different regimes, assuming $12K/J_\perp < 1$. In case of $12K/J_\perp > 1$ and $8K/J_\perp < 1$, H_1 changes to H_1^{sat} , which lies in the interval $\{H_a^{\text{sat}}, H_b^{\text{sat}}\}$ (Fig. **S3**), while for $8K/J_\perp > 1$ a spin-flip at H_a^{flip} is realized instead of the spin-flop at H_a^{flop} .

dE	Stability range	Critical field	Domain type
$E_0 - E_b^{\text{min}}$	$= \frac{M^2 H^2}{8(J_\perp + 4K)}$	$0 \leq H \leq H_a^{\text{flop}}$	$H_a^{\text{flop}} = 8/M \sqrt{K(J_\perp - 4K)}$
$E_a^{\text{min}} - E_b^{\text{min}}$	$= K \left(8 - \frac{M^2 H^2}{J_\perp^2 - 16K^2} \right)$	$H_a^{\text{flop}} \leq H \leq H_1$	$H_1 = 4/M \sqrt{(J_\perp^2 - 16K^2)/2}$
$E_a^{\text{sat}} - E_b^{\text{min}}$	$= -MH + 2J_\perp + \frac{M^2 H^2}{8(J_\perp + 4K)}$	$H_1 \leq H \leq H_a^{\text{sat}}$	$H_a^{\text{sat}} = 4/M(J_\perp - 4K)$
$E_a^{\text{sat}} - E_b^{\text{min}}$	$= -8K + \frac{\tilde{M}^2 H^2}{2(2\tilde{J} + \tilde{D} - 4K)}$	$H_a^{\text{sat}} \leq H \leq H_b^{\text{sat}}$	$H_b^{\text{sat}} = 4/M(J_\perp + 4K)$
$E_a^{\text{sat}} - E_b^{\text{min}}$	$= -8K + \frac{\tilde{M}^2 H^2}{2(2\tilde{J} + \tilde{D} - 4K)}$	$H_b^{\text{sat}} \leq H \leq H_2$	$H_2 = 4/\tilde{M} \sqrt{K(2\tilde{J} + \tilde{D} - 4K)}$
$\tilde{E}_a^{\text{min}} - \tilde{E}_b^{\text{min}}$	$= \frac{\tilde{M}^2 H^2}{2(2\tilde{J} + \tilde{D} - 4K)} - \frac{\tilde{M}^2 H^2}{2(2\tilde{J} - \tilde{D} - 4K)} + 2\tilde{D}$	$H_2 \leq H \leq \tilde{H}_a^{\text{flop}}$	$\tilde{H}_a^{\text{flop}} = 2/\tilde{M} \sqrt{(\tilde{D} + 4K)(2\tilde{J} - \tilde{D} - 4K)}$
$\tilde{E}_a^{\text{min}} - \tilde{E}_b^{\text{min}}$	$= \frac{\tilde{M}^2 H^2}{2(2\tilde{J} + \tilde{D} - 4K)} - \frac{\tilde{M}^2 H^2}{2(2\tilde{J} - \tilde{D} - 4K)} + 2\tilde{D}$	$\tilde{H}_a^{\text{flop}} \leq H \leq H_3$	$H_3 = 2/\tilde{M} \sqrt{2(\tilde{J} - 2K)^2 - \tilde{D}^2/2}$
$\tilde{E}_a^{\text{sat}} - \tilde{E}_b^{\text{min}}$	$= -2\tilde{M}H + \frac{M^2 H^2}{2(2\tilde{J} + \tilde{D} - 4K)} - 8K + 4\tilde{J}$	$H_3 \leq H \leq \tilde{H}_a^{\text{sat}}$	$\tilde{H}_a^{\text{sat}} = 2/\tilde{M}(2\tilde{J} - \tilde{D} - 4K)$
$\tilde{E}_a^{\text{sat}} - \tilde{E}_b^{\text{min}}$	$= -2\tilde{M}H + \frac{M^2 H^2}{2(2\tilde{J} + \tilde{D} - 4K)} - 8K + 4\tilde{J}$	$\tilde{H}_a^{\text{sat}} \leq H \leq \tilde{H}_b^{\text{sat}}$	$\tilde{H}_b^{\text{sat}} = 2/\tilde{M}(2\tilde{J} + \tilde{D} - 4K)$
$\tilde{E}_a^{\text{sat}} - \tilde{E}_b^{\text{sat}}$	$= -2\tilde{D}$	$\tilde{H}_b^{\text{sat}} \leq H$	-

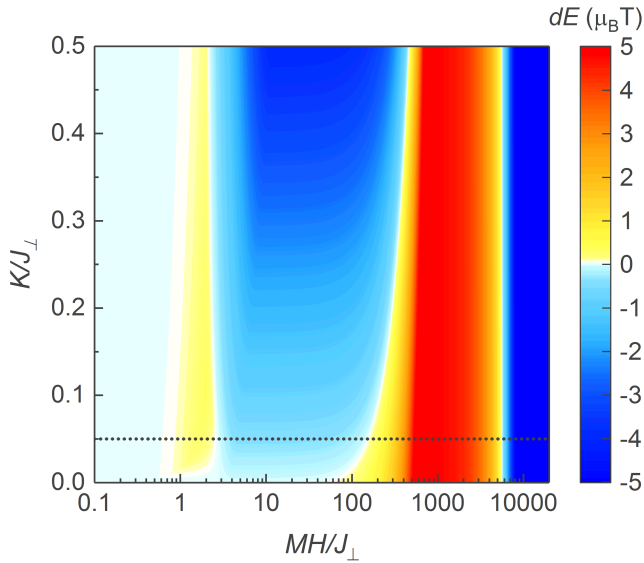


Figure **S4**: Calculated domain energy difference dE as a function of K/J_\perp and MH/J_\perp . The dotted line represents the cross section for $K/J_\perp = 0.05$ shown in Fig. (3) of the main text.

III. DETERMINING THE CONSTANTS FROM ANOTHER SET OF MEASUREMENTS

From the determination of the energy difference and the domain distribution the observed minimum (maximum) in magnetostriction, magneto-transport or field dependent neutron data around 0.4 T to 0.6 T can be associated with H_a^{flop} . As Fig. 5 in the main text illustrates, this field, at which the energy difference $|dE|$ reaches its first maximum (in the regime we are interested in) is close to the field H_0 , where the population of the b-domain starts decreasing. Thus, we can associate H_a^{flop} with H_0 and determine the relevant constants in a

different way compared to that used in the main text:

$$J_\perp = \frac{M}{4} \frac{2H_1^2 - H_0^2}{\sqrt{2(H_1^2 - H_0^2)}}$$

$$K = \frac{M}{16} \frac{H_0^2}{\sqrt{2(H_1^2 - H_0^2)}}$$

A check on the magnetoresistance data from the sample used in Zapf et al.⁵, which shows $H_0 = 0.37$ T and $H_1 = 0.64$ T (both corrected for the observed hysteresis), yields $J_\perp = 0.091$ meV and $K = 4.65$ μ eV, which are in agreement with the determination presented in the main text. See also Tab. **SII** (Sample 1). We also analyzed further samples grown with various synthesis techniques. The results are shown in Table **SII** as well.

IV. EXTRACTING THE TWIN POPULATION FROM MAGNETO-TRANSPORT DATA

Because the intrinsic resistivity of individual domains is anisotropic, and the domain population depends on

Table **SII**: Coupling constants determined from various samples and experiments. Equal superscripts in the Flux Method column indicate samples from the same batch. The corresponding data (MR, MS) in rows 2 and 3 are already published⁵. Other entries correspond to unpublished measurements.

Sample #	Measurement Technique	Flux Method	Constants [meV]		
			J_\perp	$8K$	J_\perp/K
1	$M(H)$	Fe-As ¹	0.096	0.052	14.8
1	MR	Fe-As ¹	0.091	0.036	20.0
2	MS	Bridgman ²	0.157	0.06	20.4
3	$M(H)$	Sn-flux ³	0.113	0.032	28.0
4	Neutron	Sn-flux ³	0.115	0.056	16.4
5	MR	Bridgman ⁴	0.130	0.092	11.2
6	MR	Fe-As ⁵	0.142	0.052	21.6
7	MR	Fe-As ⁵	0.135	0.108	9.8

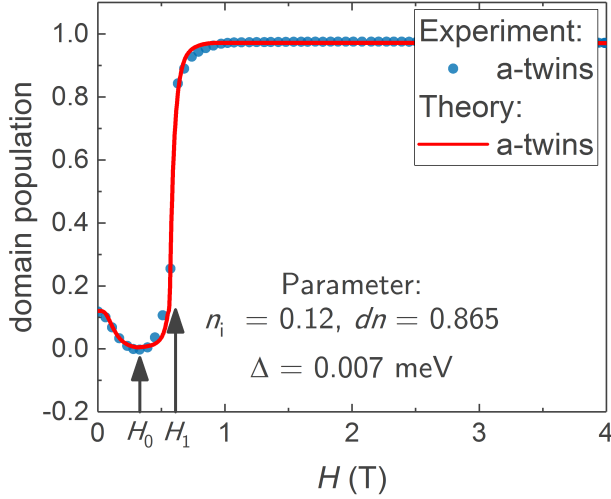


Figure **S5**: Twin domain population derived from magneto-transport⁵ at $T = 5$ K as a function of (an decreasing) magnetic field applied along the $[110]_T$ direction (blue symbols). The solid (red) line presents the theoretical prediction for the given parameters.

the magnetic field, we can extract the latter from the measured magnetoresistance (MR). In principle, the relation between MR and the twin population is nonlinear and requires solving the percolation problem. But since the intrinsic resistivity anisotropy is relatively small, this relation, whatever it is, can be linearized as if individual domains were connected in series. With this in mind, and using the fact that our neutron data (which will be published separately) show the domain ratio to saturate at high fields with $n = 0.976$, we can simply rescale the MR from Ref.⁵ as

$$n(H) = \left(1 - \frac{R(H) - R_{sat}}{R(H_0) - R_{sat}}\right) \cdot n,$$

(since the current was perpendicular to the field direction in this experiment). Here R_{sat} denotes the MR value in the saturated state above H_1 , corresponding to $n \approx 1$. The result together with a fit to the obtained data is shown in Fig. **S5**.

¹ G. Kresse, J. Hafner, Phys. Rev. B **47**, 558 (1993)

² Problems with reconciling density functional theory calculations with experiment in ferropnictides, I.I. Mazin, M.D. Johannes, L. Boeri, K. Koepernik, D.J. Singh, Phys. Rev. B **78**, 085104(R) (2008)

³ Jiang, S., Luo, Y., Ren, Z., Zhu, Z., Wang, C., Xu, X., Tao, Q., Cao, G. & Xu, Z. Metamagnetic transition in EuFe_2As_2 single crystals. New J. Phys. **11**, 025007 (2009).

⁴ Jeevan, H. S., Kasinathan, D., Rosner, H. & Gegenwart, P. Interplay of antiferromagnetism, ferromagnetism,

and superconductivity in $\text{EuFe}_2(\text{As}_{1-x}\text{P}_x)_2$ single crystals. Phys. Rev. B **83**, 054511 (2011).

⁵ Zapf, S., Stingl, C., Post, K. W., Maiwald, J., Bach, N., Pietsch, I., Neubauer, D., Löhle, A., Clauss, C., Jiang, S., Jeevan, H. S., Basov, D. N., Gegenwart, P. & Dressel, M. Persistent Detwinning of Iron-Pnictide EuFe_2As_2 Crystals by Small External Magnetic Fields. Phys. Rev. Lett. **113**, 227001 (2014).